Poly(L-lactide) (PLLA)/Multiwalled Carbon Nanotube (MWCNT) Composite: Characterization and Biocompatibility Evaluation

Donghui Zhang,[†,‡] Madhuvanthi A. Kandadai,[†] Jiri Cech,[§] Siegmar Roth,[§] and Seamus A. Curran*[,†]

New Mexico State University, Department of Physics, Las Cruces, New Mexico 88003-8001, New Mexico State University, Department of Chemistry and Biochemistry, Las Cruces, New Mexico 88003-8001, and Max Planck Institute for Solid State Research, Heisenbergstrasse 1, Stuttgart 70569, Germany

Received: March 15, 2006; In Final Form: May 8, 2006

Much effort has been directed at the fabrication of carbon nanotubes (CNTs)/polymer composites and the characterization of their physical properties. Among them, composites comprising CNTs and the biocompatible polymers are of special interest due to their potential for specific biomedical applications. We report the preparation of the MWCNT/poly(L-lactide) composite and the corresponding spectroscopic (Raman) and the microscopic (SEM, TEM) characterization. The electronic transport, thermal properties, and biocompatibility of this composite have also been investigated. The Raman spectroscopic analysis suggests the interaction between PLLA and MWCNT occurs mainly through the hydrophobic $C-CH_3$ functional groups. The DC conductivity of the composite increases as the MWCNT loading is increased. Such behavior can be described by a percolation mechanism in which a percolation threshold at about 14 wt % MWCNT loading is observed with the maximum end conductivity of 0.1 $S \cdot cm^{-1}$. The DSC study of the PLLA/MWCNT composite reveals that the MWCNTs in the composite have the effect of inducing crystallization and plasticizing the polymer matrix. The results from the cell culture test suggest that the presence of MWCNT in the composite inhibits the growth of the fibroblast cells.

Introduction

Ever since the initial discovery of carbon nanotubes (CNTs) in the 1990s,[1] much progress has been made in regard to understanding their fundamental properties.[2−5] They are known to have unique dimensional,[2] electrical,[6] and mechanical[7] properties among many others.[2,4,8] CNTs can be formally viewed as a tubular structure rolled up from a graphene sheet. Depending on the number of tubular walls, CNTs can be divided into single-walled carbon nanotubes (SWCNTs) or multiwalled carbon nanotubes (MWCNTs). SWCNTs have diameters in the range of 0.7−1.5 nm, whereas MWCNTs have diameters in the range of 2−10 nm for the innermost tubular layer and an additional thickness of ∼0.7 nm for every extra layer.[2] Different chiral vectors, which describe how the graphene sheets are rolled up, result in CNTs with different electronic structure. They can be either semiconducting or metallic.[9−11] High electrical conductivity on the order of 10^5 $S \cdot cm^{-1}$ has been reported for SWCNT ropes or films. Additionally, CNTs are known for having exceptional mechanical strength, with an estimated Young's modulus in the tetrapascal (TPa) range.[7] Yarns made of MWCNT and polymer (PVA) composite exhibited a tensile strength comparable to spider silk and a much higher toughness than spider silk, which is about five times higher than that of steel wire with the same mass.[12]

Because of the many unique properties, CNTs have demonstrated great potential to be integrated into various existing technologies such as specialty polymeric composites[8,12−16] and various electronic devices[17] such as FET,[18,19] photovoltaic,[20] organic LED,[21] field emitter,[22−25] sensors,[26,27] etc. Because of its high aspect ratio and good conductivity, CNTs are especially promising as conductive fillers for making polymeric composites with high-strength and electric-shielding properties.[28,29] A variety of commercial or noncommercial polymers have been tested as a partner material for making CNT/polymer composite.[21,28,30−37] One type of polymer that has attracted much attention lately is the biocompatible polymers such as polycaprolactone,[37,38] chitosan,[39] and polylactide.[29,40] This is largely due to the greater prospect of these materials for certain conceivable biomedical uses. For instance, an electric field is known to stimulate the healing of various tissues.[41−47] In the case of bone fracture healing, the use of an electric field was based on the observation that, when a bone was subject to mechanical loads (stress), deformation of bones (strain) is normally accompanied by an electrical signal bearing the strain characteristics.[41,42] Thus a conductive CNT-reinforced biocompatible polymer composite can potentially be used as a new-generation implant material, which could stimulate cell growth and tissue regeneration by facilitating the physioelectrical signal transfer.[48]

Among all the biopolymers, poly(L-lactide) (PLLA) is of special interest. Structurally, PLLA is a type of polyester formed from condensation of L-lactic acid or ring-opening polymerization of the cyclic diester (L-lactide).[49] Because of the presence of ester groups, it is susceptible to enzymatic and hydrolytic degradation to form L-lactic acid, a naturally occurring metabo-

* To whom correspondence should be addressed. E-mail: shay@physics.nmsu.edu.
† New Mexico State University, Department of Physics.
‡ New Mexico State University, Department of Chemistry and Biochemistry.
§ Max Planck Institute for Solid State Research.

10.1021/jp061628k CCC: $33.50
Published on Web 06/10/2006

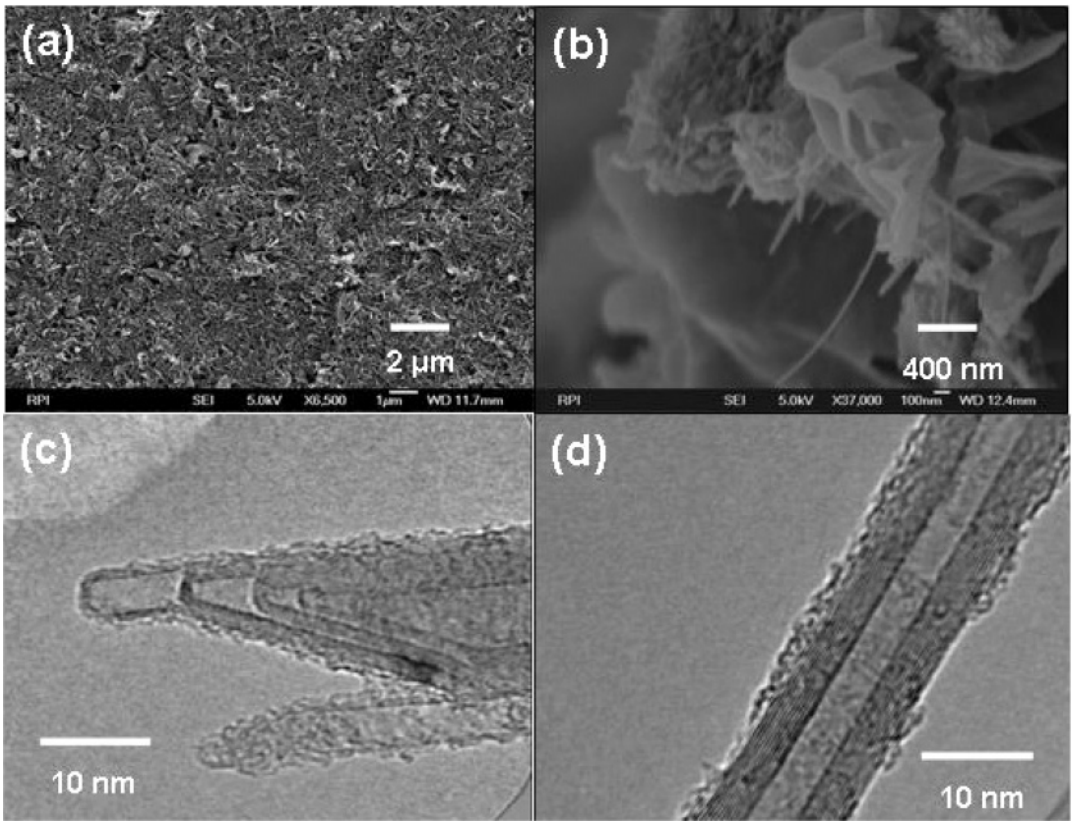

Figure 1. (a) FE-SEM image of PLLA/MWCNT composite with 3 wt % MWCNT loading; (b) magnified FE-SEM image of PLLA/MWCNT composite with 3 wt % MWCNT loading; (c, d) HR-TEM images of PLLA/MWCNT (7 wt %) composite showing PLLA absorbed on the MWCNT surface.

lite in the human body. Until very recently, PLLA has been limited to biomedical applications as resorbable implant materials (bone screw or fracture fixation plates) because of its biodegradability and high production cost. A recent innovation on the production process significantly lowered the production cost, which further stimulated the studies on its property and potential applications.[49] In this paper, we will describe the preparation, spectroscopic, and electrical characterization of poly(L-lactide)/MWCNT composite as well as results from the cell culture test to evaluate the biocompatibility of the composite material.

Results and Discussion

The PLLA/MWCNT composites with different MWCNT loadings were prepared by the solution-mixing and precipitation method, as described in the Experimental Section. The composites appear visually uniform, and the field emission scanning electron microscopy (FE-SEM) (Figure 1a, b) clearly indicates the presence of MWCNTs both on the surface of the composite as well as inside the polymer matrixes. Micrographs of the composite from high-resolution transmission electron microscopy (HR-TEM) (Figure 1c, d) also revealed the absorption of PLLA polymer on the surface of MWCNTs.

MWCNT have very distinct Raman resonances and they are highly sensitive toward immediate environmental changes. Thus, Raman spectroscopy is a very powerful tool for characterizing the interfacial interaction of a PLLA/MWCNT composite. The Raman spectra of a PLLA/MWCNT composite with 3 wt % MWCNT loading was shown in Figure 2 together with the baseline corrected Raman spectra for the purified MWCNT and purified PLLA for comparison. Under the 785 nm excitation wavelength, the PLLA sample shows strong fluorescence. The

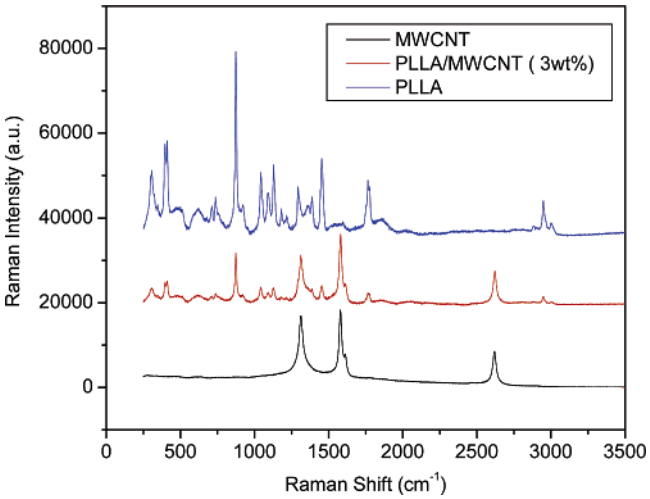

Figure 2. Baseline-corrected Raman spectra of the PLLA/MWCNT composite with 3 wt % MWCNT loading (the middle red curve), the purified MWCNT (the bottom black curve), and the purified PLLA sample (the top blue curve).

PLLA/MWCNT composite also fluoresces, but the intensity is significantly mitigated as compared to the pure PLLA sample. The presence of the MWCNTs in the composite is supported by the characteristic D, G, D′, and D* modes of MWCNTs observed at 1313.8, 1580.4, 1613.8, and 2621.5 cm^{-1}, respectively (Table S1, Supporting Information). The G mode is the symmetry-allowed tangential E_{2g} mode, where as the D and D′ modes are due to the first-order double resonance Raman scattering process and reflect the presence of structural disorders on the graphite plane of the nanotubes.[50−52] The D* mode is a second-order overtone mode and is not a disorder-induced mode.

Thus, all peaks are normalized against the D* mode prior to any intensity comparison.[53] While a 3.4 cm^{-1} blue-shift was observed for the D′ mode upon formation of composite, the D, G, and D* modes of the composite did not exhibit substantial positional shift (<1.5 cm^{-1}) as compared to the purified MWCNT itself. In terms of the relative Raman intensity normalized against the D* mode and the full width at half-maximum intensity (fwhm), the disorder-induced modes (D and D′) behaved very differently from these nondisorder-induced modes (G and D*). The relative intensity and the fwhm of the D mode and the D′ mode decreased substantially upon formation of the composite, whereas the G mode exhibited a small increase in the relative intensity and a substantial increase of the fwhm and the D* mode also displayed a small increase of fwhm (Table S1, Supporting Information). The rest of vibrational responses in the Raman spectrum of the composite correspond to different PLLA vibrational modes (Figures S1−S3, Supporting Information). Detailed assignment of corresponding modes has been reported elsewhere.[54,55] These Raman resonances due to the PLLA in the composite are much broader than these for the pure PLLA in terms of full width at half-maximum intensity (fwhm) and are not as intense as the ones due to the MWCNT. These changes might be due to the interaction between PLLA and MWCNT, which alters the resonance condition for the PLLA. Also, most of these PLLA resonances in the composite do not exhibit any positional shift (<1 cm^{-1}) as compared to the pure PLLA sample, except that the resonances due to C−CH_3 stretching (1042.3 cm^{-1}), −CH_3 rocking mode (1127.4 cm^{-1}), and −CH_3 asymmetric bending mode (1452.8 cm^{-1}) were red-shifted by 1.5, 1.9, and 1.5 cm^{-1}, respectively, from the corresponding modes (1043.8, 1129.3, and 1454.3 cm^{-1}) in the pure PLLA sample (Figures S1−S3, Supporting Information). This suggests that the interaction between the PLLA and the MWCNT occurs through the C−CH_3 group. Finally, the PLLA in the composite remains semicrystalline, as indicated by the presence of the characteristic combination mode of helical backbone vibration and −CH_3 rocking modes at 920.6 cm^{-1} as well as the splitting patterns of C═O stretching (1750−1780 cm^{-1}) and C−H stretching modes (2880−3005 cm^{-1}).[54]

Thin films of the nanocomposite were spin-cast from a dichloromethane solution. The conductivities of PLLA/MWCNT composite, as a function of MWCNT loadings, was measured on the spin-cast thin film by a two-point probe method using vacuum-deposited gold as electrodes. The plot of log (conductivity) vs MWCNT wt % (1−20 wt %) for our composites gives a single-stage percolation curve (Figure 3). Previously, in studying the percolation network of polypyrrole in a conducting polymer composite, Fourier et al.[56] analyzed the insulator-to-conductor transition according to the percolation theory and proposed an analytical model (eq 1) based on Fermi−Dirac distribution to fit the experimental data of composite conductivity, where σ_c, σ_n, and σ_p are the conductivities of the composite, nanotubes, and polymers, respectively, p is the mass fraction of the nanotubes, and b is an empirical parameter that leads to the change in conductivity at the percolation threshold (p_c).

$$\log(\sigma_c) = \log(\sigma_n) + \frac{\log(\sigma_p) - \log(\sigma_n)}{1 + e^{[b(p-p_c)]}} \qquad (1)$$

By fitting log (conductivity) of our composites at different MWCNT loadings into the eq 1, a percolation threshold (p_c) of 13.5 wt % and b value of 1.07 were derived with the maximum end conductivity of 0.1 S·cm^{-1} at ∼14 wt % or higher pristine MWCNT loadings. The conductivities of our composite are consistently lower than those previously reported by Hyon et al. at the corresponding MWCNT loadings. However, taking into account of the difference in the preparation procedure for the composite and the MWCNT source, the discrepancy in electric conductivity is not surprising. The charge transport in such composite materials is dominated by charge hopping from one conductive site to the next. Its macroscopic behavior can be described by a percolation mechanism, through which a significant increase in conductivity is typically observed once the percolative pathway is established.[57] Thus, a good dispersion of the conductive sites (MWCNTS in this case) in the polymeric matrixes is critical in terms of establishing the percolative pathway required for an efficient charge transport. Not only does it affect the percolation threshold, but also the conductivity level of the composite. Different preparation methods for the composite can significantly affect the dispersion of MWCNT in the composite and, hence, the transport properties.[58] Moreover, the aspect ratio of the conductive filler is also known to have important effect on the conductivity of the composite material. Theoretical calculations by Foygel et al. have shown that onset of percolation and the conductivity exponent was strongly dependent on the aspect ratio (a) defined by $a = l/d$, where d is the diameter and l the length,[59] and the conductivity could be changed by altering the aspect ratio in a three-dimensional system.[59] Thus, MWCNTs with a different aspect ratio from different sources might also contribute to the observed discrepancy in the transport properties.

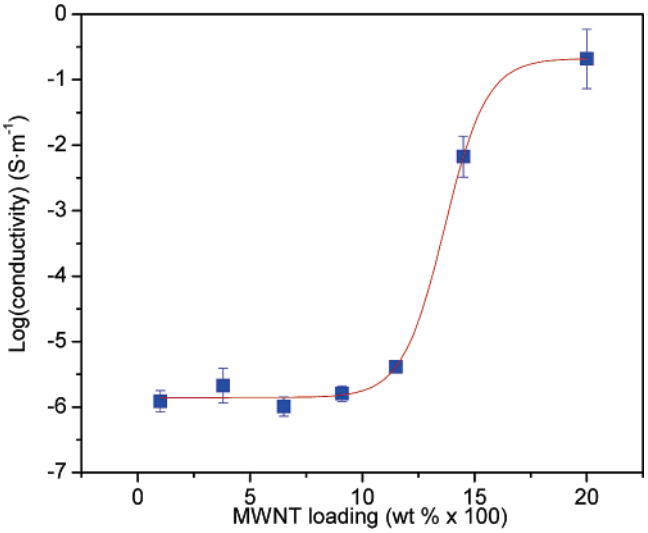

Figure 3. Semilogarithmic plot of PLLA/MWCNT composite conductivity as a function of mass fraction of MWCNT in the composite. The solid line represents a curve fit using eq 1. The parameters for the best fit are: 1 wt % ≤ p < 20 wt %; p_c = 13.5 wt %; b = 1.07.

To assess the effect of MWCNTs on the thermal behavior of PLLA matrix, the differential scanning calorimetry (DSC) experiments were conducted and the results were summarized in Table 1 and Figures S4−S5, Supporting Information. All PLLA/MWCNT (1−20 wt %) composite samples exhibited the anticipated glass transition (T_g: 59.3−62.2 °C), the crystallization exotherm (T_c: 99.1−101.6 °C), and the melting endotherm (T_m: 172.1−176.4 °C) peaks in the first heating cycle. The glass transition temperature appeared to increase slightly as the MWCNT loading increased. However, the increment is almost negligible on account of the error associated with such measurements. The crystallization temperature and the melting temperature do not exhibit any obvious correlation with the MWCNT loading. On the second heating cycle, the glass transitions of the composites were significantly broadened into the baseline

TABLE 1: Differential Scanning Calorimetry (DSC) Results for the PLLA and the PLLA/MWCNT Composites with Different Compositions

	1st heating cycle					2nd heating cycle				
MWCNT loading (%)	T_g (°C)	T_c (°C)	T_m (°C)	ΔH_c (J·g^{-1})	ΔH_m (J·g^{-1})	T_g (°C)	T_c (°C)	T_m (°C)	ΔH_c (J·g^{-1})	ΔH_m (J·g^{-1})
0	65.1	107.5	182.4	−21.9	35.7	64.3	108.5	182.2	−17.5	36.0
1	59.3	99.7	176.2	−22.4	34.7			175.4		29.7
3.8	59.7	100.6	172.1	−18.9	29.8			172.6		25.3
6.5	60.1	99.8	173.3	−21.8	37.4			174.5		30.8
9.1	60.8	101.6	175.7	−21.6	38.5			175.1		32.0
11.5			176.4		29.1			178.0		25.4
14.5	61.4	100.8	176.4	−21.8	36.5			178.1		33.4
20	62.2	99.7	173.3	−12.2	27.3			175.6		23.3

and cannot be accurately located. The crystallization exotherms also disappeared. The melting endotherm peaks were broadened, with a shoulder appearing at lower temperature, which became more prominent as the MWCNT loading was increased. Interestingly, this shoulder was not observed during the second heating cycle for the pristine PLLA sample. Therefore, we attributed the appearance of the shoulder in the melting endotherms of the composites to the formation of different type or size of PLLA crystallites. These new crystallites might form in the proximity to the MWCNTs, which are known to induce crystallization of surrounding polymers.[60,61] In addition, we also observed that the glass transition temperature (T_g,), crystallization temperature (T_c), and the melting temperature (T_m) of the composites were all notably lower than the corresponding T_g (65.1 °C), T_c (107.5 °C), and T_m (182.4 °C) of the purified PLLA sample. This observation suggests that the MWCNTs serve the role of a plasticizer and a crystal nucleate, which enhances the polymer segmental mobility and facilitates the crystal packing simultaneously.

To test cell viability on the PLLA/MWCNT composite, a simple cell culture test was performed using 10T1/2 fibroblast cell lines. The glass cover slips were spin-coated with the pure PLLA or the PLLA/MWCNT (7 wt %) composite and the plain cover slip was used as a control. After sterilization by autoclaving, an equal amount of fibroblast cells were plated onto these cover slips and incubated in Eagle's basal growth media (BME) at 37 °C over a period of 8 days, when the cell growth reaches confluence. The growth of the cells was monitored by the fluorescence microscopy and was quantified by the cell counts per unit area. The detailed procedure is provided in the Experimental Section.

Through the microscopic observation over the period of the cell growth, the cells were found to be uniformly distributed over all the covers slips and typical fibroblast morphology with cellular projections was observed (Table S2, Supporting Information). Phase contrast imaging on cover slips from day 1 and day 3 showed that the cells lay flat on the surface of the cover slips. This reflects the overall good adherence of the cells to the surface of the cover slips. The cell cytoplasm was of uniform size until the cell growth reached confluence. Thereafter, the cell cytoplasm appeared smaller in size due to lack of space. There was no change in the size of the nuclei of the cells when observed with fluorescent imaging.

The cell attachment and proliferation were evident on the control, the PLLA coated, and the PLLA/MWCNT (7 wt %) coated cover slips. However, the degree of cell growth is significantly dependent on the coating type. Detailed cell density changes over a period of 8 days are summarized in Table 2 and Figure 4. The growth of the fibroblast cells on the control and the PLLA-coated cover slips followed a similar profile, whereas the cell growth on the PLLA/MWCNT (7 wt %) cover slip was somewhat impeded. Various factors can contribute to the

TABLE 2: Fibroblast Cell Counts Per Unit Area on the Control, the PLLA Coated, the PLLA/MWCNT (7 wt %) Coated Cover Slips at the Different Incubation Intervals[a]

	day1	day 3	day 6	day 8
control	6 ± 1	38 ± 9	121 ± 19	218 ± 23
PLLA	3 ± 1	40 ± 8	114 ± 19	207 ± 23
PLLA/MWCNT	5 ± 1	27 ± 4	72 ± 26	146 ± 54

[a] The error bar was based on 95% confidence level.

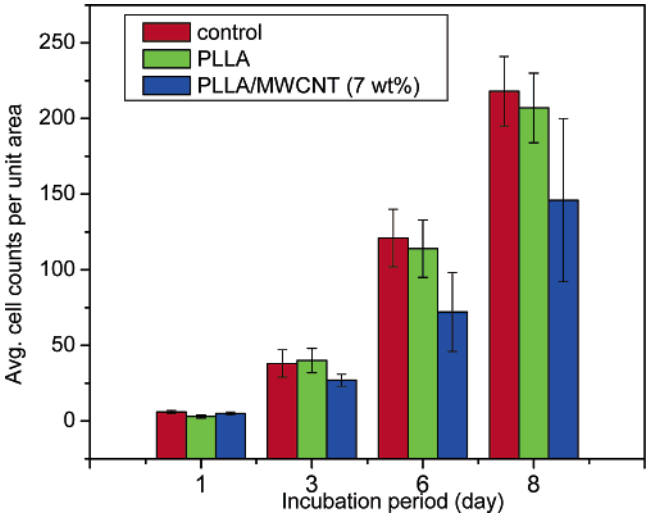

Figure 4. Fibroblast cell counts per unit area on the control, the PLLA coated, and the PLLA/MWCNT (7 wt %) coated cover slips at the different incubation intervals.

difference in the growth profile of fibroblast cells. At this stage, we are not able to deduce the specific contributing factors for the relatively slow growth of fibroblast cells on our PLLA/MWCNT composite surface. However, under microscopic observation, the surface of the PLLA/MWCNT coated cover slips was noticeably less smooth with many crater-shaped bumps. It has been previously observed that the carbon nanotubes tend to aggregate within the hydrophobic region of the lipid bilayer of the cell membrane. A high concentration of carbon tubes can destabilize or even cause rupture of the membrane.[62] Thus, it is plausible that anchoring of the fibroblast cells on the PLLA/MWCNT composite surface might be inhibited due to the unfavorable interaction between the cell membrane and MWCNTs that penetrate out of the composite surface. Further investigation into the role of carbon nanotubes on the cell growth and viability is needed and well warranted in view of the increasing amount of interest in applying CNTs for biomedical purposes.

Conclusion and Summary

We have reported the preparation of a poly(L-lactide) and MWCNT composite through a simple solution blending and

precipitation method. The composite was characterized by Raman spectroscopy, FE-SEM, and HR-TEM. The Raman spectroscopic analysis suggests the interaction between PLLA and MWCNT occurs through the more hydrophobic $C-CH_3$ groups. The DC transport properties of the composite can be described by a percolation mechanism, in which a percolation threshold at about 14 wt % MWCNT loading was observed with the maximum end conductivity of 0.1 $S \cdot cm^{-1}$. While the conductivity values are lower than that reported elsewhere, the discrepancy is due to the different levels of dispersion of the MWCNT in the polymer matrixes as well as the potential aspect ratio difference of the MWCNTs. The study of the PLLA/MWCNT composite by the differential scanning calorimetry (DSC) reveals that the MWCNTs in the composite has the effect of plasticizing the PLLA matrix, which results in the lower T_g, T_c, and T_m than those of the pristine PLLA. The appearance of a shoulder for the melting endotherm peak on the second heating cycle suggested the formation of new crystallites, which is likely to be induced in the proximity of MWCNTs. The results from the cell culture test suggest that the presence of MWCNT in the composite inhibits the growth of the fibroblast cells. The exact reason for this inhibition is not yet clear, although the less-favorable attachment of the cells to the PLLA/MWCNT composite surface might be a plausible cause.

Experimental Section

Equipment. The Raman spectra were collected on a Renishaw Raman spectrometer. The excitation source at 785 nm was generated using the 785 nm diode laser with maximum power of 380 mW. The Raman band of silicon (520 cm^{-1}) was used to calibrate the spectrometer, with a resolution better than 1.5 cm^{-1}. Raman samples were prepared by spin-casting the sample suspension onto a silicon wafer. All spectra were normalized against the D* mode when the relative peak intensities are in discussion. Relevant peak parameters were obtained by least-squares fitting of Lorentzian line shapes to the measured spectra. The DC conductivity measurement was done using a two-point probe setup with vacuum deposited gold as electrodes. The SEM images were obtained from a Zeiss55 Supra, and high-resolution field emission SEM (FE-SEM) was performed at 5 kV. High-resolution TEM (HR-TEM) was performed on a Philips CM200 microscope with a point resolution of 0.27 nm, operated at an acceleration voltage of 200 kV, equipped with LaB6 source. The PLLA/MWCNT sample was dispersed in dichloromethane and drop cast onto a copper grid with a holey Lacey carbon film. The sample was allowed to dry at ambient temperature for 2 min and was then heated at 75 °C for 15 min prior to high-resolution transmission electron microscopy (HR-TEM) study. Differential scanning calorimetry (DSC) was performed on a Perkin-Elmer PYRIS I instrument. An indium/gallium standard was used for calibration, and the argon was used as the purge gas. The Hoechst 33342 stained fibroblast cell samples from the minimum essential medium (MEM) test were analyzed at a 200× magnification with a Zeiss Axiovert 200M microscope equipped with a CCD fluorescent camera.

Materials. Methanol, anhydrous DMF, dichloromethane, acetone, sulfuric acid, and nitric acid were purchased from Aldrich and were used as received without further purification. The poly(L-lactide) (PLLA) pellets (Aldrich, $M_w = 100-150$ $kg \cdot mol^{-1}$) were purified by dissolution in dichloromethane and subsequent precipitation in an excess of methanol. The precipitated PLLA was filtered and dried in a vacuum at 80 °C overnight. Multiwalled carbon nanotubes (MWCNTs) prepared by arc discharge method were purchased from SES Research and purified by an acid-treatment process to remove residual catalyst and amorphous carbons. This involves sonication (130 W) of MWCNTs (100 mg) in concentrated H_2SO_4/HNO_3 (70:30 v/v, 10 mL) for 12 h. The suspension was filtered under vacuum through a nylon Whatman microfilter (0.2 μm pore size) and washed thoroughly with distilled water until a neutral pH was obtained. The sample was then washed thoroughly with ample acetone and dried at 60 °C under vacuum overnight. To conduct the cell culture test, the glass cover slips (Fisher brand, 18 mm diameter) were purchased from Fisher Scientific. C3H/10T1/2 mouse embryonic (fibroblast) cell lines were purchased from the American Type Culture Collection (ATCC, Manassas, Virginia) and grown in Eagle's basal growth media (BME) (Invitrogen, Carlsbad, CA) supplemented with 10% fetal bovine serum and 2 mM L-glutamine at 37 °C in a humidified atmosphere of 95% air and 5% CO_2. Hoechst 33342 (Molecular Probes, Carlsbad, CA) was used as received to stain the cell nuclei.

Procedures. The polymer blend was prepared through a solution mixing. The amount of MWCNTs was adjusted to give the desired MWCNT loading. A representative procedure is as follows. A DMF (1 mL) suspension of MWCNT (50 mg) and purified PLLA (200 mg) was stirred in a round-bottom flask at 110 °C under N_2 overnight. The black suspension was poured into an excess of methanol, and the precipitate was filtered, washed with methanol, and dried at 100 °C under vacuum overnight to afford a fluffy black solid (226 mg, 90% yield).

A representative procedure for the cell culture test is as follows. The purified PLLA (9 mg) was dissolved in dichloromethane (10 mL) and was spin-coated onto a glass cover slip at 3000 rpm for 10 s. The PLLA/MWNT (7 wt %) composite sample (4 mg) was dissolved in dichloromethane (11 mL) and was spin-coated onto a cover slip at 3000 rpm for 10 s. Cover slips coated with either the PLLA or the PLLA/MWNT composite were prepared in the same manner. The plain glass cover slips with no coatings were used as controls. All glass cover slips (coated or noncoated) were autoclaved at a temperature of 120 °C for 45 min prior to the plating of cells. This includes 30 min of sterilization and 15 min of drying. An equal number of 10T1/2 fibroblast cell lines was plated onto the cover slips, and equal amounts of Eagle's basal growth media were added to each of the wells. The wells were incubated at 37 °C to allow the growth of fibroblast cells, which was monitored over a period of 8 days. After the growth for 1, 3, 6, and 8 days, the fibroblast cells in parallel wells were fixed, stained with the DAPI, and analyzed through a fluorescence microscope. Fluorescence images from 10 different unit areas of the cover slip were taken. The number of cells were counted for each area and averaged to provide an estimation of the cell density on each cover slip. The error bar was obtained by the standard statistic analysis with a 95% confidence level.

A representative DSC experimental procedure is as follows. A small amount of the polymer or polymer composite was loaded onto an aluminum pan with a cover. In the DSC experiment, the sample was heated rapidly from the ambient temperature to 150 °C at a rate of 40 $C \cdot min^{-1}$, whereupon the temperature was held for 10 min to remove all thermal history. The sample was then cooled to 0 °C at a rate of 40 $C \cdot min^{-1}$, where the temperature was held for another 10 min before heating to 180 °C at a rate of 10 $C \cdot min^{-1}$. The glass transition temperature (T_g) was determined from the first heating scan by a mathematical averaging method. Straight lines were fit tangent to the heat flow curve before and after the transition. From the

average of the slopes and intercepts of these two lines, a third line was obtained and the T_g was taken as the temperature at which the heat flow curve intersected this third line. The crystallization temperature (T_c) and the melting temperature (T_m) were also determined from the first heating scan and the second heating scan if the corresponding transition occurred. T_m and T_c were taken as the temperatures corresponding to the melting peak maximum or crystallization peak minimum. ΔH_c and ΔH_m were taken as the corresponding integrated peak areas divided by the heating rate and the sample weight.

Acknowledgment. Dr. Curran gratefully acknowledges ARC AFSOR 106427. Dr. Zhang acknowledges the NSF-ADVANCE program (NSF0123690) for partial financial support. Jiri Cech acknowledges International Max Planck Research School for Advanced Materials (IMPRS-AM) for financial support. We acknowledge Dr. Pulickel M. Ajayan and Victor Pushparaj (RPI) for conducting SEM experiments as well as the INBRE-supported Cell and Organismal Culture Facility and the technical assistance of Hyun-Jung Kim in the cell culture experiments.

Supporting Information Available: Expanded Raman spectra of the PLLA, the MWCNT and the PLLA/MWCNT (3 wt %) composite; a table for the MWCNT Raman responses in the PLLA/MWCNT (3 wt %) composite; the differential scanning calorimetry (DSC) traces of the PLLA/MWCNT composite (1−20 wt %), the PLLA and the MWCNT samples; phase contrast images of fibroblast cells on cover slips coated the PLLA/MWCNT (7 wt %) composite and the purified PLLA respectively as well as the control surface over the 8-day growth period. This material is available free of charge via the Internet at http://pubs.acs.org.

References and Notes

(1) Iijima, S. *Nature* **1991**, *354*, 56.
(2) Saito, R.; Dresselhaus, G.; Dresselhaus, M. S. *Physical Properties of Carbon Nanotubes*; Imperial College Press: London, 1999.
(3) Ouyang, M.; Huang, J.; Lieber, C. M. *Acc. Chem. Res.* **2002**, *35*, 1018.
(4) Dresselhaus, M. S.; Dresselhaus, G.; Charlier, J. C.; Hernández, E. *Philos. Trans. R. Soc. London, Ser. A* **2004**, *362*, 2065.
(5) Kastner, J.; Pichler, T.; Kuzmany, H.; Curran, S.; Blau, W.; Weldon, D. N.; Delamesiere, M.; Draper, S.; Zandbergen, H. *Chem. Phys. Lett.* **1994**, *221*, 53.
(6) Tans, S. J.; Devoret, M. H.; Dai, H.; Thess, A.; Smalley, R. E.; Geerligs, L. J.; Dekker, C. *Nature* **1997**, *386*, 474.
(7) Treacy, M. M. J.; Ebbesen, T. W.; Gibson, J. M. *Nature* **1996**, *381*, 678.
(8) Baughman, R. H.; Zakhidov, A. A.; de Heer, W. A. *Science* **2002**, *297*, 787.
(9) Ugawa, A.; Rinzler, A. G.; Tanner, D. B. *Phys. Rev. B* **1999**, *60*, R11305.
(10) Itkis, M. E.; Niyogi, S.; Meng, M. E.; Hamon, M. A.; Hu, H.; Haddon, R. C. *Nano Lett.* **2002**, *2*, 155−159.
(11) Ouyang, M.; Huang, J.-L.; Cheung, C. L.; Lieber, C. M. *Science* **2001**, *292*, 702.
(12) Dalton, A. B.; Collins, S.; Muñoz, E.; Razal, J. M.; Ebron, V. H.; Ferrais, J. P.; Coleman, J. N.; Kim, B. G.; Baughman, R. H. *Nature* **2003**, *423*, 703.
(13) Lahiff, E.; Ryu, C. Y.; Curran, S.; Minett, A. I.; Blau, W.; Ajayan, P. M. *Nano Lett.* **2003**, *3*, 1333.
(14) Coleman, J. N.; Curran, S. A.; Dalton, A. B.; Davey, A. P.; McCarthy, B.; Blau, W.; Barklie, R. C. *Synth. Met.* **1999**, *102*, 1174.
(15) Curran, S.; Davey, A. P.; Coleman, J.; Dalton, A.; McCarthy, B.; Maier, S.; Gray, D.; Brennan, M.; Ryder, K.; de la Chapelle, M. L.; Journet, C.; Bernier, P.; Byrne, H. J.; Carroll, D.; Ajayan, P. M.; Lefrant, S.; Blau, W. J. *Synth. Met.* **1999**, *103*, 2559.
(16) Dalton, A. B.; Byrne, H. J.; Coleman, J. N.; Curran, S.; Davey, A. P.; McCarthy, B.; Blau, W. *Synth. Met.* **1999**, *102*, 1176.
(17) Rao, S. G.; Huang, L.; Setyawan, W.; Hong, S. *Nature* **2003**, *425*, 36.
(18) Park, J. G.; Kim, G. T.; Park, J. H.; Yu, H. Y.; McIntosh, G.; Krstic, V.; Jhang, S. H.; Kim, B.; Lee, S. H.; Lee, S. W.; Burghard, M.; Roth, S.; Park, Y. W. *Thin Solid Films* **2001**, *393*, 161.
(19) Star, A.; Gabriel, J.-C. P.; Bradley, K.; Gruner, G. *Nano Lett.* **2003**, *3*, 459.
(20) Ago, H.; Petritsch, K.; Shaffer, M. S. P.; Windle, A. H.; Friend, R. H. *Adv. Mater. (Weinheim, Ger.)* **1999**, *11*, 1281.
(21) Curran, S. A.; Ajayan, P. M.; Blau, W. J.; Carroll, D. L.; Coleman, J. N.; Dalton, A. B.; Davey, A. P.; Drury, A.; McCarthy, B.; Maier, S.; Strevens, A. *Adv. Mater. (Weinheim, Ger.)* **1998**, *10*, 1091.
(22) de Heer, W. A.; Châtelain, A.; Ugarte, D. *Science* **1995**, *270*, 1179.
(23) Wang, Q. H.; Corrigan, T. D.; Dai, J. Y.; Chang, R. P. H.; Krauss, A. R. *Appl. Phys. Lett.* **1997**, *70*, 3308.
(24) Sharma, R. B.; Tondare, V. N.; Joag, D. S.; Govindaraj, A.; Rao, C. N. R. *Chem. Phys. Lett.* **2001**, *344*, 283.
(25) Jung, Y. J.; Kar, S.; Talapatra, S.; Soldano, C.; Viswanathan, G.; Li, X.; Yao, Z.; Ou, F. S.; Avadhanula, A.; Vajtai, R.; Curran, S.; Nalamasu, O.; Ajayan, P. M. *Nano Lett.* **2006**, *6*, 413.
(26) Stetter, J. R.; Maclay, G. J. *Adv. Micro. Nanosyst.* **2004**, *1*, 357.
(27) Joshi, K. A.; Tang, J.; Haddon, R.; Wang, J.; Chen, W.; Mulchandani, A. *Electroanalysis* **2005**, *17*, 54.
(28) Ma, C. M.; Huang, Y.; Kuan, H.; Chiu, Y. *J. Polym. Sci., Part B: Polym. Phys.* **2005**, *43*, 345.
(29) Moon, S.; Jin, F.; Lee, C. H.; Tsutsumi, S.; Hyon, S. *Macromol. Symp.* **2005**, *224*, 287.
(30) Zhu, J.; Kim, J.; Peng, H.; Margrave, J. L.; Khabashesku, V. N.; Barrera, E. V. *Nano Lett.* **2003**, *3*, 1107.
(31) Sandler, J.; Shaffer, M. S. P.; Prasse, T.; Bauhofer, W.; Schulte, K.; Windle, A. H. *Polymer* **1999**, *40*, 5967.
(32) Allaoui, A.; Bai, S.; Cheng, H. M.; Bai, J. B. *Compos. Sci. Technol.* **2002**, *62*, 1993.
(33) Lin, Y.; Rao, A. M.; Sadanadan, B.; Kenik, E. A.; Sun, Y.-P. *J. Phys. Chem. B* **2002**, *106*, 1294.
(34) Kong, H.; Gao, C.; Yan, D. *J. Am. Chem. Soc.* **2004**, *126*, 412.
(35) Lin, Y.; Zhou, B.; Fernado, K. A. S.; Liu, P.; Allard, L. F.; Sun, Y.-P. *Macromolecules* **2003**, *36*, 7199.
(36) Qin, S.; Qin, D.; Ford, W. T.; Resasco, D. E.; Herrera, J. E. *Macromolecules* **2004**, *37*, 752.
(37) Lou, X.; Detrembleur, C.; Sciannamea, V.; Pagnoulle, C.; Jérôme, R. *Polymer* **2004**, *45*, 6087.
(38) Buffa, F.; Hu, H.; Resasco, D. E. *Macromolecules* **2005**, *38*, 8258.
(39) Wang, S.; Shen, L.; Zhang, W.; Tong, Y. *Biomacromolecules* **2005**, *6*, 3067.
(40) Chen, G.; Kim, H.; Park, B.; Yoon, J. *J. Phys. Chem. B* **2005**, *109*, 22237.
(41) Aaron, R. K.; Ciombor, D. M. *J. Cell. Biochem.* **2004**, *52*, 42.
(42) Ciombor, D. M.; Aaron, R. K. *J. Cell. Biochem.* **1993**, *52*, 37.
(43) Aaron, R. K.; Ciombor, D. M. *J. Cell. Biochem.* **1993**, *52*, 42.
(44) Goldman, R.; Pollack, S. *Bioelectromagnetics* **1996**, *17*, 450.
(45) Politis, M. J.; Zanakis, M. F. *Neurosurgery* **1989**, *25*, 71.
(46) Pomeranz, B.; Campbell, J. J. *Brain Res.* **1993**, *603*, 271.
(47) Sisken, B.; Walker, J.; Orgel, M. *J. Cell. Biochem.* **1993**, *51*, 404.
(48) Supronowicz, P. R.; Ajayan, P. M.; Ullmann, K. R.; Arulanandam, B. P.; Metzger, D. W.; Bizios, R. *J. Biomed. Mater. Res.* **2002**, *59*, 499−506.
(49) Drumright, R. E.; Gruber, P. R. *Adv. Mater.* **2000**, *12*, 1841.
(50) Saito, R.; Grüneis, A.; Samsonidze, G. G.; Brar, V. W.; Dresselhaus, G.; Dresselhaus, M. S.; Jorio, A.; Cançado, L. G.; Fantini, C.; Pimenta, M. A.; Souza Filho, A. G. *New J. Phys.* **2003**, *5*, 157.1.
(51) Tan, P.; An, L.; Liu, L.; Guo, Z.; Czerw, R.; Carroll, D. L.; Ajayan, P. M.; Zhang, N.; Guo, H. *Phys. Rev. B* **2002**, *66*, 245410.
(52) Chakrapani, N.; Curran, S.; Wei, B.; Ajayan, P. M.; Carrillo, A.; Kane, R. S. *J. Mater. Res.* **2003**, *18*, 2515.
(53) Curran, S. A.; Talla, J. A.; Zhang, D.; Carroll, D. L. *J. Mater. Res.* **2005**, *20*, 3368.
(54) Kister, G.; Cassanas, G.; Vert, M.; Pauvert, B.; Térol, A. *J. Raman Spectrosc.* **1995**, *26*, 307.
(55) Qin, D.; Kean, R. T. *Appl. Spectrosc.* **1998**, *52*, 488.
(56) Fourier, J.; Boiteax, G.; Seytre, G.; Marichy, G. *Synth. Met.* **1997**, *84*, 839.
(57) Coleman, J. N.; Curran, S. A.; Dalton, A. B.; Davey, A. P.; McCarthy, B.; Blau, W. J.; Barklie, R. C. *Phys. Rev. B* **1998**, *58*, R7492.
(58) Curran, S. A.; Zhang, D.; Wondmaqegn, W. T.; Ellis, A. V.; Cech, J.; Roth, S.; Carroll, D. L. *J. Mater. Res.* **2005**, in press.
(59) Foygel, M.; Morris, R. D.; Anez, D.; French, S.; Sobolev, V. L. *Phys. Rev. B* **2005**, *71*, 104201.
(60) Levi, N.; Czerw, R.; Xing, S.; Iyer, P.; Carroll, D. L. *Nano Lett.* **2004**, *4*, 1267.
(61) Li, C. Y.; Li, L.; Cai, W.; Kodjie, S. L.; Tenneti, K. K. *Adv. Mater.* **2005**, *17*, 1198.
(62) Nimmagadda, A.; Thurston, K.; Nollert, M. U.; McFetridge, P. S. *J. Biomed. Mater. Res.* **2006**, *76A*, 614.